A Mathematical Model for Heterogeneous Reactions with a Moving Boundary

A general mathematical model is presented for the noncatalytic reaction between a porous solid and a gas with solid product formation under conditions controlled by intraparticle diffusion. The model has been formulated in general terms so as to allow the incorporation of specific details pertaining to actual systems. The formulation assumes that the gaseous reactant diffuses through the pore space of the particle followed by diffusion through the product layer. The resulting equations are solved numerically.

This model has been used to predict conversion-time curves for the atmospheric oxidation of iron disulfide contained in porous solids. The predicted curves are in excellent agreement with the experimental data. In particular, it produces accurate estimates for the conversion rates of iron disulfide at different temperatures.

Kareem I. Batarseh
Glenn P. Swaney
Alfred H. Stiller
Department of Chemical Engineering
West Virginia University
Morgantown, WV

Introduction

Heterogeneous reactions involving the formation of a solid product are of considerable importance in many industrial, chemical, and metallurgical processes. Examples are the roasting of sulfide and the like, reduction of iron ores to metal, calcination of sulfides to make oxides, and the regeneration of catalysts. Such heterogeneous reactions are fairly complex, and their complete analysis involves a large number of physical and chemical rate processes. These complications arise from the deposition of the solid product on the surface of the reacting solid. Thus, the gaseous reactant must diffuse through this layer to react with unreacted solid.

In recent years there has been a growing interest in the development of mathematical models that describe the above reaction systems for use in gas-solid reactor design or analysis of experimental reactivity data. The general subject has been reviewed by Szekely et al. (1976). More specifically, the development of the grain model (Szekely and Evans, 1970) has provided an effective tool for the analysis of noncatalytic gas-solid reactions with a solid product. A critical review of the available information on the modeling of gas-solid reactions has been compiled by Ramachandran and Doraiswamy (1982). In this comprehensive review, three common models pertaining to gas-solid reactions are discussed, as well as the stability of such systems and the type of experimental data required for modeling. Weisz and Goodwin (1963) studied the combustion reaction of carbonaceous fuel such that the reaction rate is controlled by diffusion. In this case, the analysis becomes identical to the shrinking-core model.

Gibson and Harrison (1980) have applied the shrinking-core model to the reaction of H_2S with ZnO. In their study, all the model parameters were determined experimentally except for the effective diffusivity of the reactant gas in the product layer, which was obtained from the model solutions. Tseng, Tamhankar and Wen (1981) studied the reactions of iron sulfide with oxygen and sulfur dioxide. The experiments were carried out under the conditions of complete control by chemical or diffusion kinetics. Their data have been interpreted based on the grain model.

A random pore model in the kinetically controlled regime for a fluid-solid reaction was developed by Bhatia and Perlmutter (1980). In a following article (1981), the authors extended the earlier model to incorporate inter- and intraparticle transport effects. The model accounted for structural changes of the solid matrix, which were assumed to result from a random overlapping of a set of cylindrical surfaces. Numerical predictions indicated qualitative agreement of the model with experimental observations.

Davis and Ritchie (1986) in a recent paper have developed a mathematical model to describe the oxidation of iron disulfide with oxygen. In this model, oxygen supply was assumed to be by

Current address of K. I. Batarseh is P.O. Box 191, Amman, Jordan.
Correspondence concerning this paper should be addressed to A. H. Stiller.

diffusion through the pore space of the particles constituting the bed, followed by diffusion toward a moving reaction front within the particles. Basically, the model was a set of coupled differential equations with a moving boundary. The particles were assumed to be spherically shaped and the reaction front within these particles was assumed to behave like the shrinking-core model.

In general the above models neglect the intraparticle diffusion resistance of the gaseous reactant through the pores of the particles as being unimportant with the consequent assumption that the gaseous reactant concentration within each particle is constant. This greatly simplifies the problem. Since this assumption is invalid in some cases, it is important to solve the problem by including this effect.

The main objective of the present study is to formulate a model for gas-solid systems under isothermal conditions which incorporates the product layer resistance to diffusion but couples the effect of diffusion within the pores of the particles. The analysis will again be based on the previously adopted picture of a porous solid (Szekely et al., 1976) as being made up of small reactant grains identical to the shrinking-core model assumption, but reaction of these grains is not uniform throughout the particle. In addition, no allowance is made for structural changes, and interparticle diffusion effects are neglected.

Also, this paper presents the results of a numerical solution to the model equations, as applied to the oxidation of FeS_2 in rock samples which produce acid mine drainage. Our laboratory studies have produced a substantial quantity of experimental data on this heterogeneous reaction system. Most of these experiments have been carried out under strong intraparticle diffusion limitations.

Model Development

We consider porous particles of radius R_o such that each particle contains a distribution of small grains of solid (B), of initial radius r_o. Let the distance from the center of the particles (macroscopic radial coordinate) be r, and the distance from the center of the grains (microscopic radial coordinate) be r'. This is show schematically in Figure 1.

Species A diffuses through the surrounding fluid phase (gas or liquid), and the pores and reacts with B on the interior pore surface of the particles according to the general stoichiometry

$$aA_{(g)} + bB_{(s)} \rightarrow cC_{(s)} + fF_{(g,l)} \tag{1}$$

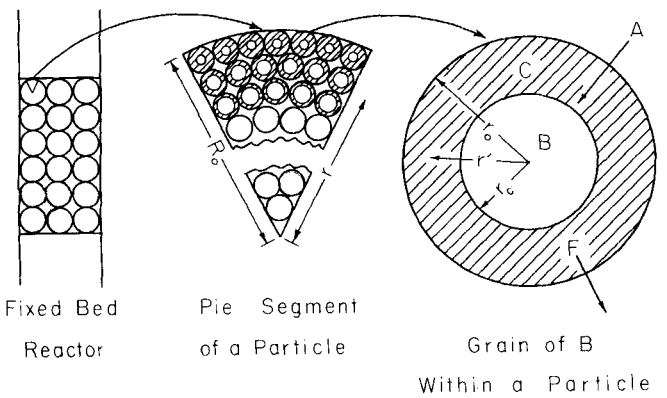

Figure 1. Schematic representation of the model.

The reaction of each grain is assumed to proceed from the outside surface toward the center of the grains, so that the reaction front within each grain exhibits spherical symmetry.

Because of the formation of solid C, a progressively thicker solid product layer at radius r_c covers the reactive surface. The domain $r_o - r_c$ is referred to as the "ash layer," through which the gaseous reactant A must diffuse to reach fresh B. Hence, during the reaction, the solid reactant is characterized by two portions:

1) An unreacted core of B which shrinks as the reaction proceeds
2) A reacted shell of product

Thus, the term "shrinking unreacted core" is used to describe this scenario.

The development of the present model is based on the assumption that the grains present at the surface of the particles are more accessible to gaseous A than the ones embedded within the particles. Therefore, the conversion of solid B is a function of both time and macroscopic radial position. It is assumed further that the concentration of A exceeds the required stoichiometric ratio necessary for the reaction with B. This assumption implies that a significant concentration gradient of A exists only within the particle itself. Also, the model assumes that the system is isothermal and the size of the particles remains constant during the reaction.

Model Formulation

For clarity, the derivation of the model can be divided into three steps. The first step describes the accessibility of A to the reacting solid grains embedded in the particles. The second step of the model describes the resulting change of the grains of B as the reaction proceeds. The third step combines the functional representations in Steps I and II to give an overall system of equations to determine the rate of solid conversion.

Step I. A steady-state material balance on species A, describing the diffusion in the pores within a particle can be written as:

$$\frac{\partial}{\partial r}(r^2 N_A) - S_v r^2 N'_A|_{r'=r_o} = 0 \tag{2}$$

where

N_A = flux of A within the particle

$N'_A|_{r'=r_o}$ = flux of A within the grain "ash layer"

Here $S_v = (3\rho_b)/(r_o \rho_B) \cdot w$, the grain surface area per unit volume of particle, ρ_b is the bulk density of the particles, ρ_B is the density of the solid, w is the weight fraction of B in the sample. Equation 2 is written as a partial differential equation because N_A and N'_A are functions of both radial position and time.

Assuming low concentrations of A, N_A can be represented in terms of Fick's law and an overall effective diffusion coefficient, $\mathcal{D}_e$; thus, Eq. 2 becomes

$$\mathcal{D}_e C_M \frac{\partial}{\partial r}\left(r^2 \frac{\partial y_A(r,t)}{\partial r}\right) = -S_v r^2 N'_A|_{r'=r_o} \tag{3}$$

where

C_M = molar density of the fluid (gas or liquid) within the particle

y_A = mole fraction of gas A dissolved in fluid M

Equation 3 is subject to the following boundary conditions:

$$\forall t > 0 \text{ at } r = R_o: \quad y_A = y_{A\infty} \tag{4}$$

and

$$\forall t > 0 \text{ at } r = 0: \quad \frac{\partial y_A}{\partial r} = 0 \tag{5}$$

where $y_{A\infty}$ is the concentration of gas A at the surface of the particle. The derivation of Eq. 4 assumes that the resistance to external mass transport is negligible. Also, since we assume that the inert structural matrix is unaffected by the reaction, the porosity and consequently the effective diffusivity, $\mathcal{D}_e$, are constant.

A mass balance on A within the "ash layer," $r_o - r_c$, can be expressed as

$$\frac{\partial}{\partial r'}\left(r'^2 \frac{\partial y'_A(r_c, r, t)}{\partial r'}\right) = 0 \tag{6}$$

subject to the boundary conditions

$$\forall t > 0 \text{ at } r' = r_c: \quad y'_A = 0 \tag{7}$$
(diffusion controlled kinetics)

$$\forall t > 0 \text{ at } r' = r_o: \quad y'_A = y_A \tag{8}$$

Equation 7 implies an instantaneous reaction, and Eq. 8 links the macroscopic (particle) and microscopic (grain) concentrations of A at the surface of the grains.

The assumptions inherent in Eq. 6 are homogeneity of the spherical grain, constant effective diffusivity, and the pseudo-steady state approximation, i.e., that the unreacted core is stationary. This approximation has been examined critically by Bischoff (1963) who concluded that for gas-solid reactions, the pseudo-steady state assumption is reasonable in describing real situations.

By integrating Eq. 6 twice and using the boundary conditions, the concentration of A within the grain can be expressed by:

$$y'_A(r_c, r, t) = \frac{y_A(r, t)}{\left(1 - \dfrac{r_c(r, t)}{r_o}\right)}\left(1 - \frac{r_c(r, t)}{r'}\right) \tag{9}$$

This equation relates the concentration of A within the grains to the one in the pores and implicitly to time.

Step II. The next step is to relate the shrinking of the core to the reaction rate, and hence, to y'_A. The rate of consumption of solid B is given by

$$\frac{\partial r_c(r, t)}{\partial t} = \frac{\bar{b}}{C_B} N'_A|_{r'=r_c} = -\frac{\bar{b}}{C_B} C_F \mathcal{D}'_e \left(\frac{\partial y'_A(r_c, r, t)}{\partial r'}\right)\Bigg|_{r'=r_c} \tag{10}$$

with the initial condition

$$\text{at } t = 0: \quad r_c = r_o \tag{11}$$

Here, C_B and C_F are the molar densities of reactant B and fluid F respectively; $\bar{b}$ is the stoichiometric ratio relating consumption of B and A, $\bar{b} = b/a$ (see Eq. 1), and $\mathcal{D}'_e$ is the effective diffusivity of A within the reacted shell.

Step III. Equations 9 and 10 are sufficient to establish r_c in terms of t and y_A. To obtain this result, Eq. 9 is first differentiated with respect to r', evaluated at $r' = r_c$, and then substituted into Eq. 10:

$$\left(1 - \frac{r_c(r, t)}{r_o}\right) r_c(r, t) \frac{\partial r_c(r, t)}{\partial t} = -\frac{\bar{b}}{C_B} C_F \mathcal{D}'_e y_A(r, t) = -\Omega y_A(r, t) \tag{12}$$

with the initial condition

$$\text{at } t = 0 \quad 0 \le r \le R_o \quad r_c = r_o \tag{13}$$

In order to relate the concentration of gaseous reactant A in the pores of the particles to the conversion rate of the solid B, Equation 10 is substituted into Eq. 3 to eliminate

$$N'_A|_{r'=r_o} = \frac{r_c^2}{r_o^2} N'_A|r'=r_c$$

from the expression; hence,

$$\frac{1}{r^2}\frac{\partial}{\partial r}\left(r^2 \frac{\partial y_A(r, t)}{\partial r}\right) = -\eta \frac{\partial r_c(r, t)}{\partial t} \cdot r_c^2 \tag{14}$$

with the boundary conditions

$$\forall t > 0 \quad \text{at } r = R_o \quad y_A = y_{A\infty} \tag{15}$$

$$\forall t > 0 \quad \text{at } r = 0 \quad \frac{\partial y_A}{\partial r} = 0 \tag{16}$$

where

$$\eta = \frac{S_v C_B}{\bar{b} \mathcal{D}_e C_M r_o^2}$$

The final system of Eqs. 12–16 now define a physically reasonable model describing the diffusion and the reaction of species A within the particles.

Equations 12 through 16 do not give r_c explicitly as a function of r and t because the functional dependence of y_A on r and t is not clear. Thus, solution at this point is not possible. However, this difficulty can be overcome by introducing a new function $\phi(r, t)$ having the form

$$\phi(r, t) = \int_0^t y_A(r, t)\, dt \tag{17}$$

Integrating the above equations with respect to time and using

Leibnitz's rule for differentiation of integrals, one obtains

$$\frac{1}{r^2}\frac{\partial}{\partial r}\left(r^2\frac{\partial\phi(r,t)}{\partial r}\right) = -\frac{\eta}{3}\left(r_c^3(r,t) - r_o^3\right) \tag{18}$$

$$3r_c^2(r,t) - \frac{2r_c^3(r,t)}{r_o} - r_o^2 + 6\Omega\phi(r,t) = 0 \tag{19}$$

$$\forall t > 0 \quad \text{at } r = R_o: \quad \phi = y_{A\infty}t \tag{20}$$

$$\forall t > 0 \quad \text{at } r = 0: \quad \frac{\partial\phi}{\partial r} = 0 \tag{21}$$

Since $\phi(r, t)$ is known as a function of r_c from Eq. 19, r_c can be found by substituting this quantity into Eqs. 18, 20 and 21. Expressing the final system in nondimensional form,

$$\frac{1}{Z^2}\frac{\partial}{\partial Z}\left(Z^2\left[Y^2(Z,t) - Y(Z,t)\right]\frac{\partial Y(Z,t)}{\partial Z}\right) = -\frac{\theta}{3}\left[Y^3(Z,t) - 1\right] \tag{22}$$

Boundary conditions:

$$\forall t > 0 \quad \text{at } Z = 1: \quad 1 + 2Y^{*3} - 3Y^{*2} = \beta t \tag{23}$$

$$\forall t > 0 \quad \text{at } Z = 0: \quad \frac{\partial Y}{\partial Z} = 0 \tag{24}$$

where

$$Z = \frac{r}{R_o}$$

$$Y = \frac{r_c}{r_o}$$

$$Y^* = Y(Z = 1, t)$$

$$\theta = \eta\Omega r_o R_o^2 = \frac{3\rho_b\mathcal{D}'_e R_o^2 C_F w}{\rho_B\mathcal{D}_e r_o^2 C_M}$$

$$\beta = \frac{6\Omega}{r_o^2}y_{A\infty} = \frac{6\bar{b}y_{A\infty}C_F\mathcal{D}'_e}{r_o^2 C_B}$$

Equations 22–24 are valid for $0 \le Z \le 1.0$, provided that Y is never zero. However, when $Y = 0$, i.e., the grains are completely reacted in that region, one has to modify the equations as well as the boundary conditions. The time required for complete conversion at the surface can be obtained by substituting $Y^* = 0$ into Eq. 23; the result can be expressed as:

$$\text{at } Z = 1.0: \quad \mathcal{T} = 1/\beta \tag{25}$$

Now as the reaction proceeds from the surface of the particle toward the center, there exists for $t > \mathcal{T}$ a moving boundary, $Z^*(t)$, which separates two regions $Z^* \le Z \le 1.0$ (where $Y = 0$), and $0 \le Z \le Z^*$ (where $Y \ne 0$), denoted by I and II, respectively. All the grains within Region I are completely reacted, while those within II are not.

Equations 22–24 can be solved to obtain conversions for $t < \mathcal{T}$; however, complications arise when $t > \mathcal{T}$ since the solution depends on $Z^*(t)$. We therefore proceed to derive the equations needed to determine this unknown moving boundary.

Where the conversion of the solid is completed in the particle, Eq. 18 can be written in terms of Z for $Z^* < Z < 1.0$ as:

$\forall t > \mathcal{T}$ at $Z^* < Z < 1.0$:

$$\frac{1}{Z^2}\frac{\partial}{\partial Z}\left(Z^2\frac{\partial\phi_I(Z,t)}{\partial Z}\right) = \frac{\eta}{3}r_o^3 = 2y_{A\infty}\theta\mathcal{T} \tag{26}$$

The boundary conditions can be obtained from Eq. 19, where $r_c = 0$, and Eq. 20; hence,

$$\forall t > \mathcal{T} \quad \text{at } Z = Z^*: \quad \phi_I = \frac{r_o^2}{6\Omega} = y_{A\infty}\mathcal{T} \tag{27}$$

and

$$\forall t > \mathcal{T} \quad \text{at } Z = 1.0: \quad \phi_I = y_{A\infty}t \tag{28}$$

The solution of the above system is simply

$$\phi_I(Z, t > \mathcal{T}) = \frac{1}{3}y_{A\infty}\theta\mathcal{T}\left[Z^2 - 1\right] + y_{A\infty}t + \alpha(Z^*, t)\left[1 - \frac{1}{Z}\right] \tag{29}$$

where

$$\alpha(Z^*, t) = \frac{y_{A\infty}Z^*}{(Z^* - 1)}\left[\frac{1}{3}\theta\mathcal{T}\left(1 - Z^{*2}\right) - t + \mathcal{T}\right] \tag{30}$$

In Region II, one must solve Eq. 18 subject to the boundary conditions given by Eqs. 21 and 27. Note that Eq. 27 is used for both regions, since at the moving boundary, the concentrations of A in Regions I and II must be the same.

An additional boundary is required; here we utilize the fact that the mass flux of the diffusing species is continuous at Z^*, namely

$$\forall t > \mathcal{T} \quad \text{at } Z = Z^*: \quad \frac{\partial\phi_I}{\partial Z} = \frac{\partial\phi_{II}}{\partial Z} \tag{31}$$

The above equation is used by Carslaw and Jäger (1959) to deal with an analogous heat transfer problem. Also, similar classical problems which make use of this boundary condition have been discussed by Crank (1975).

Differentiating Eqs. 27 and 29 with respect to Z and substituting the result into Eq. 31 yields

$$\forall t > \mathcal{T}: \quad 1 + 2Z^{*3} - 3Z^{*2} = \frac{3}{\theta}\left(\frac{t}{\mathcal{T}} - 1\right) \tag{32}$$

For finite θ, the time required for complete conversion of the particle, $\mathcal{T}_c$, can be deduced by noting that Z^* will be 0 in Eq. 32:

$$\mathcal{T}_c = \left(\frac{\theta}{3} + 1\right)\mathcal{T} \tag{33}$$

It is important to note that for complete conversion of the grains at the surface, the times obtained from Eqs. 25 and 32 are identical.

Examining Eqs. 23 and 32, one can observe the striking resemblance between the two forms. However, in the latter equation, the effect of intraparticle diffusion is introduced through the parameter θ. This result is not unexpected since at any region within the particle, there are diffusional resistances caused by both intraparticle and ash layer effects. On the other hand, at the surface only ash layer diffusion is present, keeping in mind the assumption of negligible interface mass transfer resistance stated earlier.

For all times, the overall conversion, X, can be obtained by integrating over the particle:

$$X(t) = 1 - 3\int_0^1 Z^2 Y^3(Z, t)\, dZ \tag{34}$$

The dimensionless radius of the unreacted grain core, $Y(Z, t)$, (and hence the conversion, X) can be determined as a function of time and radial coordinate, once the above equations are solved.

Solution Procedure

The system of partial differential equations (Eqs. 12 and 14) are initially very stiff due to the instantaneous reaction and the absence of a controlling "ash layer." The transformation function given by Eq. 17 and the application of Leibnitz's Rule reduced this system of partial differential equations to a single ordinary differential equation (Eq. 22), which is sensitive to the parameter θ, but considerably easier to integrate than Eqs. 12 and 14. However, an analytical solution to Eq. 22 does not appear possible in light of the highly nonlinear term. Therefore, Eqs. 22–24 were solved numerically using the fourth-order Runge-Kutta method; the computer program used can be found elsewhere (Batarseh, 1987).

Application of this algorithm requires that Eq. 22 be decomposed into two first-order differential equations using the following definitions:

$$\frac{\partial Y}{\partial Z} = P \tag{35}$$

$$\frac{\partial P}{\partial Z} = -\frac{\theta}{3}\frac{(Y^2 + Y + 1)}{Y} - \left[\frac{(2Y - 1)}{(Y^2 - Y)}\frac{\partial Y}{\partial Z} + \frac{2}{Z}\right]\frac{\partial Y}{\partial Z} \tag{36}$$

For slow diffusion rates or short times, the grains near the center of the particle remain completely unreacted. This requires that the boundary conditions given by Eq. 24 be modified to

$$\forall t > 0 \quad \text{at } Z = 0 \quad \text{or } Y = 1: \quad \frac{\partial Y}{\partial Z} = 0 \tag{37}$$

This modified boundary condition effectively eliminates the initial stiffness mentioned earlier; in essence, it assumes that there will still be a thin, controlling diffusional film surrounding the grains which are completely unreacted. Application of L'Hopital's Rule, where appropriate, yields the following alternative forms to Equation 36:

$$\lim_{Z\to 0}\frac{\partial P}{\partial Z} = \frac{1}{3}\left[\frac{-\theta}{3}\frac{(Y^2 + Y + 1)}{Y} - \frac{(2Y - 1)}{(Y^2 - Y)}\left(\frac{\partial Y}{\partial Z}\right)^2\right] \tag{38}$$

$$\lim_{Y\to 1}\frac{\partial P}{\partial Z} = \frac{1}{3}\left[\frac{-\theta}{3}\frac{(Y^2 + Y + 1)}{Y} - \frac{2}{(2Y - 1)}\left(\frac{\partial Y}{\partial Z}\right)^2 - \frac{2}{Z}\left(\frac{\partial Y}{\partial Z}\right)\right] \tag{39}$$

$$\lim_{\substack{Y\to 1\\ Z\to 0}}\frac{\partial P}{\partial Z} = \frac{1}{5}\left[\frac{-\theta}{3}\frac{(Y^2 + Y + 1)}{Y} - \frac{2}{(2Y - 1)}\left(\frac{\partial Y}{\partial Z}\right)^2\right] \tag{40}$$

The solution algorithm proceeds as follows:

I. The parameters θ and β are specified by the problem.

II. Equation 22 is integrated from $Z = 0$, $Y = 1$, radially outward until $Z = 1$ or $Y = 0$. This establishes the value of Y^* or Z^* for which the grains at the center have just begun to react, i.e., when the concentration profile of A has just broken through the center of the particle.

III. If Step II resulted in a value for Y^*, integration starts at $Z = 0$ and $0 < Y < 1$, otherwise integration starts at $0 < Z < 1$ and $Y = 1$. Integration proceeds radially outward until $Z = 1$ or $Y = 0$. The initial Y or Z value is adjusted and integration repeated until the final values $Z^* = 1$ and $Y^* = 0$ are simultaneously reached. This establishes the initial Y and Z values which correspond to the time $\mathcal{T}$.

IV. A time of interest is selected and Eq. 23 ($t < \mathcal{T}$) or Eq. 32 ($t > \mathcal{T}$) is solved by Newton's method to determine the appropriate boundary Y^* or Z^*. These equations have only one real root between 0 and 1.

V. The results of Steps II–IV allow the appropriate region of initial Y or Z values to be bracketed. Within this region, the initial Y or Z is adjusted until integration terminates at Y^* or Z^*, as the case may be. These iterations, like those in Step III, employ the secant method.

VI. On the final iteration, the integral of Eq. 34 is simultaneously performed using Simpson's Rule. If the integration did not start at $Z = 0$, Y values of the unreacted particle core are taken to be unity.

Only Steps IV–VI are repeated for additional times of interest. To ensure acceptable accuracy, integrations were performed using 10,000 steps. Since the complete integration procedure for one time of interest required less than 3 minutes to run on a VAX 11/785, no attempt was made to optimize the step size. However, the results were spot-checked for accuracy by doubling the number of steps.

Typical computed conversion profiles as a function of radial distance at different times are drawn in Figure 2 for $\theta = 3$. For illustrative purposes, θ was chosen so that $\mathcal{T}_c = 2\mathcal{T}$. This figure not only shows the shape of the conversion profiles, but also the times for complete conversion of the particles ($\beta t = 2$), and of the grains at the surface ($\beta t = 1$). Also, it depicts the motion of the moving boundary, $Z^*(t)$, at different times.

Model Parameters

In order to obtain conversion-time behavior, it is necessary to evaluate the parameters θ and β. Besides the measured parame-

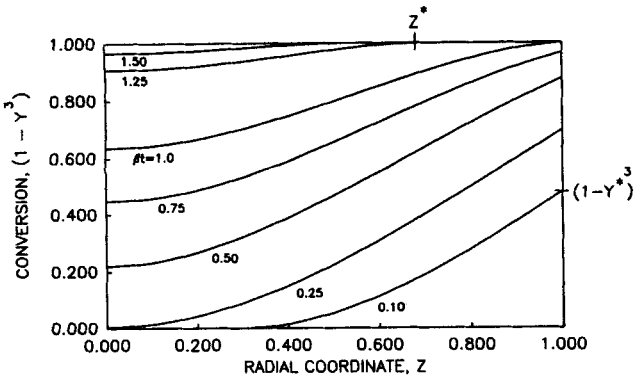

Figure 2. Conversion of grains vs. radial position for $\theta = 3$ at various times.

ters, the concentration of A at the surface of the particle ($y_{A\infty}$), as well as the effective diffusivities $\mathcal{D}_e$ and $\mathcal{D}'_e$ must be evaluated.

It is noted that for our model, interparticle diffusion resistance is assumed negligible. Thus, the gaseous concentration ($y_{A\infty}$) is the same as that in the bulk fluid surrounding the particles.

In general, if A is diffusing through a gas (M or F), the effective diffusivities $\mathcal{D}_e$ and $\mathcal{D}'_e$ depend on both bulk and Knudsen diffusion regimes. For the estimation of $\mathcal{D}_e$ and $\mathcal{D}'_e$, the so-called "dusty-gas" model proposed by Mason and coworkers (1967) can be used. According to this model, the effective diffusivity may be estimated using the following relationship:

$$\frac{1}{\mathcal{D}_e} = \frac{\tau}{\epsilon}\left(\frac{1}{\mathcal{D}_{AM}} + \frac{1}{\mathcal{D}_K}\right) \tag{41}$$

where $\mathcal{D}_K$ and $\mathcal{D}_{AM}$ are the Knudsen and molecular diffusivities of A in M, respectively. The molecular diffusivity can be evaluated with the aid of the Hirschfelder, Bird, and Spotz (1949) correlation, while the Knudsen diffusivity can be obtained from the equation of Evans, Watson, and Mason (1961). However, if the diffusion is in a liquid medium (M or F), Knudsen diffusion does not occur, and the molecular diffusivity can be estimated from the Wilke and Chang correlation (1955).

Before proceeding further, an important point should be made concerning the effective diffusivities of both A-M and A-F systems. The porosities of the particles, ϵ, and the product layer, ϵ', as well as the tortuosities of both the particles, τ, and the grains, τ', have to be determined before estimating $\mathcal{D}_e$ and $\mathcal{D}'_e$. The porosity of the particles can be readily determined using the helium-mercury method (Satterfield, 1970). However, complications come from determining ϵ', τ, and τ'. Since these structural parameters are difficult to obtain experimentally, except for the range of tortuosity, numerical values must be assigned. Nonetheless, the number of unknown parameters can be reduced to two (ϵ' and τ) by assuming the tortuosity to be the same in both the particle and the ash.

If the ultimate objective is to predict the effect of physical and chemical parameters on the time required to attain a certain extent of reaction, arbitrary values can be selected. This will make the results specific to these given sets of parameters. Nonetheless, the results are likely to show certain general trends that one might expect for such systems. However, in comparing between model predictions and experimental data, some of these parameters can be evaluated from empirical formulae presented in the literature (Sandry and Stevenson, 1970; Abbasi and Evans, 1983). Since these correlations are not applicable for all cases, the porosity (ϵ') and tortuosities may be considered as adjustable parameters. When fitting these to experimental data, the allowable range of tortuosities must be restricted to 2–20 (Satterfield, 1970). The values of both porosity and tortuosity which minimize the error between calculated and observed conversions are chosen.

Before we substantiate the validity of the model, let us at this point examine the effects of β and θ on the solution. From a physical viewpoint, the parameter β can be regarded as a quantity specifying the conversion of the solid reactant at the surface for a given time. Thus, it effectively scales the time coordinate of the solution (see Eqs. 23 and 32). On the other hand, the constant θ can be regarded as the ratio of the time constant for diffusion of A through the pores of the particle and through the product layer. Figure 3 shows the conversion $(1 - Y^3)$ as a function of radial position for a variety of θ values given in Eq. 22. This figure shows the tendency for the conversion to decrease with increasing θ for a given surface conversion (β and t are specified, see Eq. 23). A large value of θ, therefore, indicates that gaseous A diffuses slowly within the particle and rapidly within the product layer formed on the surface of the grains. Consequently, the diffusion of A through the pores of the particle is the rate controlling step for the advancement of the reaction front rather than through the pores of the grains for the case of small θ. As a result, penetration of A is not expected for large θ and conversion rates are low. It is also noted from Figure 3 that when $\theta = 0$, the profile is flat. This can be attributed to the fact that the diffusion of A within the particle is infinite; hence, the conversion rate is not a function of radial position.

Experimental Work

The accuracy of the mathematical model presented in this work cannot be established unless it is tested against experimental data. The atmospheric oxidation of FeS_2 in four different rock samples which produce acid mine drainage was chosen as the system for this study; this reaction proceeds according to

$$FeS_{2(s)} + \frac{7}{2}O_{2(g)} \rightarrow FeSO_{4(s)} + SO_{3(g)} \tag{42}$$

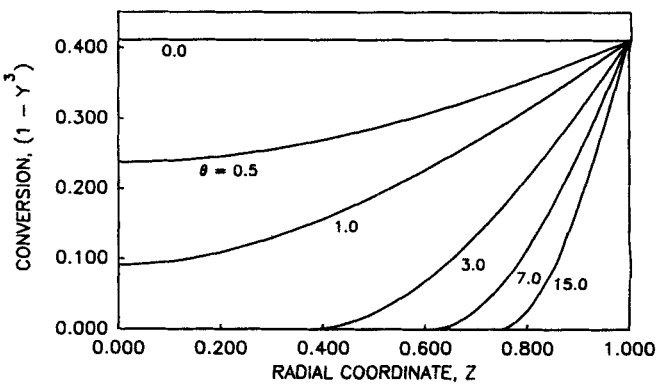

Figure 3. Conversion of solid B vs. radial position for various values of θ; $\beta t = 0.07$.

For this system, then, the fluid M is liquid water, which reacts instantly with the SO_3 product (F) to form sulfuric acid.

Here we shall confine ourselves to a brief outline of the experimental work, since full details are available elsewhere (Batarseh, 1987). Since this reaction is very slow, analysis by TGA is not feasible. Instead, the conversion rates of FeS_2 in these rocks were determined by controlled oxidation in air for specific time periods under isothermal conditions. The experiments were run at 25, 47 and 60°C, and 1 atm. The oxidation products were leached with distilled water, and the leachates were analyzed. The concentration of sulfate was chosen as the analytical parameter to monitor the amount of acid produced, because other metal ions, iron in particular, hydrolyze and effect pH measurements. The sulfate present in the leached solution was taken as a direct measurement of the amount of iron disulfide oxidized because all the sulfur produced came from the oxidation reaction.

In order to obtain higher conversions, an additional experiment was conducted at 25°C under 9.0 MPa of oxygen saturated with water vapor. A 13.5 × 10 cm ID reactor equipped with temperature, pressure and adequate safety monitoring systems was used in this study.

Ten 23-g portions from Sample 54 were inserted into the reactor to be oxidized for varied time intervals until 100% conversion was achieved. During shutdown the reactor was depressurized, following which one sample was removed to determine the conversion versus time response by the procedure stated above.

Preliminary Work

One might question the rather high solubility of $FeSO_4$ in water, since this fact would appear to contradict a fundamental model assumption. However, Eq. 42 indicates that the fluid medium surrounding the grains is not water, but concentrated sulfuric acid. Furthermore, X-ray diffraction patterns of the product in the present study showed that $FeSO_4$ is present in its monohydrated form (szomolnikite). The solubility of szomolnikite in sulfuric acid is quite low and was determined in our laboratory to be 1.5×10^{-5} g/cm^3.

It should be emphasized that the samples presented in this work have different iron disulfide morphologies and mixtures. In an attempt to study the intrinsic kinetics of the reaction and hence the morphologies, these samples were crushed to a size of 110 μm. It was found that differences in reactivities of these samples were statistically insignificant. Hence, the intrinsic reactivity can be considered independent of the type and nature of the samples used.

Experiments at various operating temperatures and for different particle sizes indicated that the reaction of FeS_2 with oxygen and water is diffusion-controlled. Apparently the oxidation of FeS_2 proceeds very rapidly at the oxygen-iron disulfide grain interface; but, oxygen diffuses slowly through both the pores of the particle and the reaction product of ferrous sulfate-sulfuric acid mixture formed on the surface of the grains.

Our knowledge of the actual macro/microstructure of the samples is quite limited, and can be summarized by the following typical values:

Particle radius	0.12 cm
Grain radius	0.005 cm (electron micrograph)
Pore radius	200 Å (mercury porosimetry)
Porosity	0.08 (helium-mercury method)

These values indicate that a grain will typically have access to many pores; hence, the assumption of constant oxygen concentration at the surface of the grains is justified.

Helium-mercury measurements of porosity as a function of time have shown only small changes (15% maximum). Thus, structural changes of the porous matrix can be neglected, and average porosity values can be used. Consequently, the effective diffusivities within both the particle and the reacted zone can be considered constant during the reaction.

Results and Discussion

The detailed data used for calculating the relevant parameters (θ and β) that appear in the model equations are given in Table I for the three experimental temperatures (25, 47 and 60°C). The data reported here have been compiled from two experimental studies (Batarseh, 1987; Haines, 1987). Physical properties such as viscosity, density, and Henry's Law constants (used in evaluating $y_{A\infty}$) were obtained from the literature (Perry and Chilton, 1973).

Although we have assumed isothermal conditions in the development of the mathematical model, the calculated conversion-time results strongly depend on the temperature through the dependence of the parameters β and θ. As a result, the sensitivity of the system's behavior to temperature is also studied by

Table 1. Physical Properties and Calculated Parameters used in the Theoretical Predictions

T = 25°C	T = 47°C	T = 60°C
C_F = 0.0186 mol/cm^3 C_B = 0.0417 mol/cm^3 C_M = 0.0554 mol/cm^3 H_A = 4.46 × 10^4 atm μ_F = 22 cp μ_M = 0.95 cp	C_F = 0.0184 mol/cm^3 C_B = 0.0417 mol/cm^3 C_M = 0.0550 mol/cm^3 H_A = 5.64 × 10^4 atm μ_F = 13 cp μ_M = 0.62 cp	C_F = 0.0183 mol/cm^3 C_B = 0.0417 mol/cm^3 C_M = 0.0546 mol/cm^3 H_a = 6.29 × 10^4 atm μ_F = 9 cp μ_M = 0.48 cp

Sample No.	ρ_b/ρ_B	w	r_o cm	S_v cm^{-1}	ϵ	β d^{-1}	θ	β d^{-1}	θ	β d^{-1}	θ
12	0.48	0.027	0.0097	4.01	0.11	9.37×10^{-6}	0.0227	1.33×10^{-5}	0.0248	1.80×10^{-5}	0.0280
44	0.49	0.015	0.0066	3.34	0.10	1.99×10^{-5}	0.0300	2.89×10^{-5}	0.0334	3.89×10^{-5}	0.0374
38	0.44	0.034	0.0032	14.03	0.050	8.47×10^{-5}	0.520	1.22×10^{-4}	0.580	1.66×10^{-4}	0.648
54	0.49	0.032	0.0019	24.80	0.091	2.42×10^{-4}	0.858	3.48×10^{-4}	0.954	4.69×10^{-4}	1.07

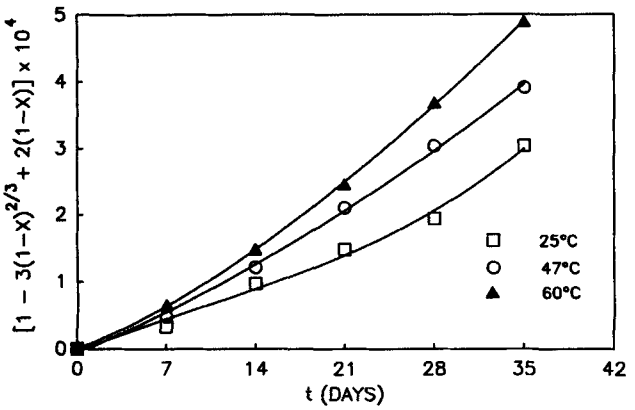

Figure 4. Conversion data according to the shrinking-core model for sample number 12.

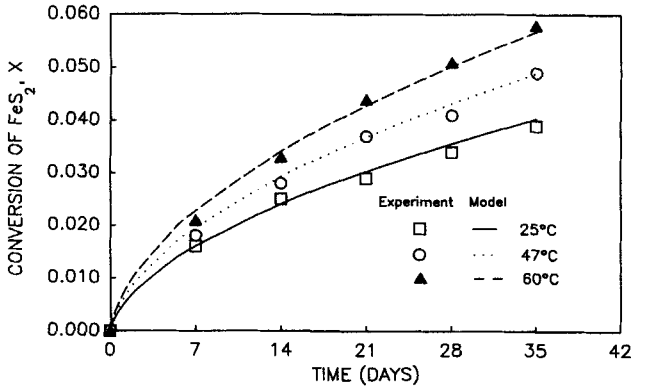

Figure 6. Experimental data vs. the model prediction for sample number 44.

comparing model predictions with actual experimental data at three different temperatures. The hidden temperature variation of the diffusivity ratio $\mathcal{D}_e'/\mathcal{D}_e$ arises because the fluid in the ash layer is concentrated H_2SO_4, while that in the pores is H_2O. This affects the diffusivities through the viscosity, molecular weight, and association parameter of the fluid.

Let us at this point examine the relative conversion data for the oxidation of FeS_2, X, in terms of the shrinking-core model (SCM). According to this model, the conversion-time relation in the pore diffusion controlled regime for a sphere can be written as (Szekely, 1976):

$$1 - 3(1 - X)^{2/3} + 2(1 - X) = \bar{t}t \qquad (43)$$

where

$$\bar{t} = \frac{6\bar{b}\mathcal{D}_e C_{A\infty}}{R_o^2 C_B}$$

The experimental oxidation data can be analyzed utilizing Eq. 43. This comparison is presented in Figure 4, where experimental conversion measurements, X, at 25, 47, and 60°C are plotted in terms of the lefthand side of Eq. 43 as a function of time for Sample 12. Clearly the SCM does not describe the experimental behavior in that the plots are non-linear through the origin. Moreover, back-calculation of the effective diffusivity, and hence, τ from the slopes of the plots gives a value for τ of about 1,620, which is unrealistic considering the range of values presented in the literature (Satterfield, 1970). The disagreement found can be attributed to the fact that the SCM does not account for the diffusion in both the pores and the ash layer, which should give a lower effective diffusivity. This decrease in effective diffusivity is indicated by the extremely large value of the tortuosity predicted by the SCM. Therefore, it can be concluded that the shrinking-core model is inappropriate for this system.

On the other hand, Figures 5–8 show typical sets of computed curves obtained by the numerical solution of Eqs. 22–24, as well as the experimental data. These figures depict the conversion of FeS_2 as a function of time, at various temperatures for four different samples. By examining the above figures, it is seen that there is generally an excellent agreement between measurements and model predictions over quite a range of temperatures. It may be noted that the experimental conversion-time curve of FeS_2, X, increases rapidly at first and then increases slowly until it levels off. This behavior is clearly depicted by the numerical solution. It is important to note that in obtaining the numerical solution the same values of the tortuosity (τ or τ') and the porosity of the ash layer, ϵ', were used for all the runs. The value of τ or τ' thus found was 10, and the corresponding ϵ' was 0.02. These values were adjusted by the method suggested previously. It is apparent that the values of tortuosity and porosity are rather

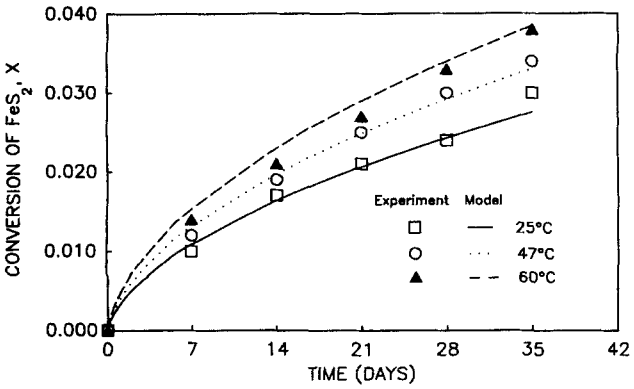

Figure 5. Experimental data vs. the model prediction for sample number 12.

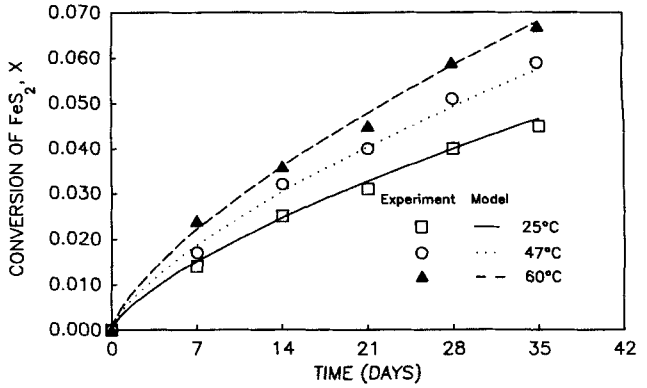

Figure 7. Experimental data vs. the model prediction for sample number 38.

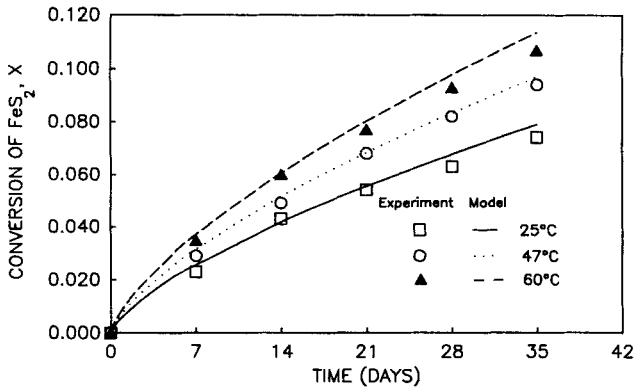

Figure 8. Experimental data vs. the model prediction for sample number 54.

high and low, respectively. This can be attributed to the fact that the product $FeSO_4 \cdot H_2O$ is dense and has low porosity. Since the porosity of the ash is comparable to that of the particles, this substantiates the assumption of equal tortuosities within the pores and the grains.

To achieve higher conversions, one has to increase the pressure, thereby increasing the solubility of oxygen in water, $y_{A\infty}$. This conclusion can be substantiated by examining Eq. 33. The time required for complete conversion, $\mathcal{T}_c$, is inversely proportional to $y_{A\infty}$ through $\mathcal{T}$, and directly proportional to θ. The underlying difficulty in decreasing θ comes from two sources:

1) For $\theta \ll 3$, the dominant term in the numerator of Eq. 33 is independent of θ.

2) Since the reaction is mass-transfer-controlled, θ cannot be varied significantly with temperature or pressure.

Increasing $y_{A\infty}$ on the other hand, does contribute to the reduction of $\mathcal{T}_c$.

Agreement of numerical results with experimental data which attained complete conversion is shown in Figure 9, with the calculated values of θ and β given in the legend. For quantitative purposes, all parameters are fixed at the values shown in Table 1 for Sample 54 at 25°C, except the solubility of oxygen, which was 1.93×10^{-3} mol O_2/mol H_2O (Zoss et al., 1954). Figure 9 demonstrates an excellent agreement in behavior of the theoretical curve with the data, showing a consistent trend throughout the entire conversion range. The solution of the model equations has therefore allowed us to describe accurately

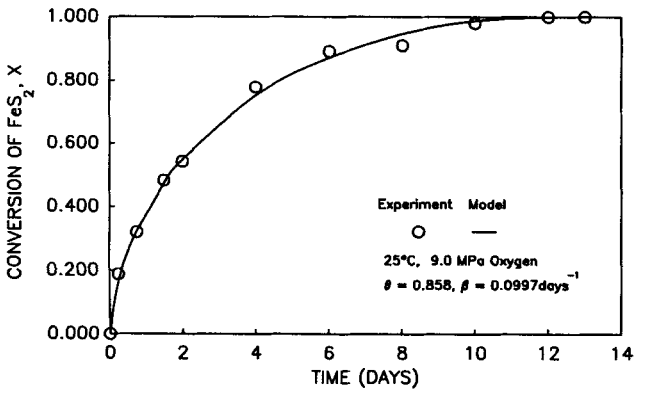

Figure 9. High-pressure oxidation data vs. the model prediction for sample number 54.

the motion of the moving boundary and conversion profiles for this system.

Notation

A = gas reactant
a = stoichiometric coefficient
B = solid reactant
b = stoichiometric coefficient
$\bar{b}$ = stoichiometric ratio relating consumption of A and B, $\bar{b} = b/a$
C = solid product
c = stoichiometric coefficient
$C_{A\infty}$ = molar concentration of reactant gas at the surface of the particle
C_B = molar density of solid reactant B
C_F = molar density of fluid product F
C_M = molar density of the fluid within the particle
$\mathcal{D}_{AM}$ = molecular diffusivity of gas A in fluid medium M
$\mathcal{D}_e$ = effective diffusivity of gas A within the pores of the particle
$\mathcal{D}'_e$ = effective diffusivity of gas A within the reacted shell
$\mathcal{D}_K$ = Knudsen diffusivity of gas A
F = fluid product
f = stoichiometric coefficient
H_A = Henry's constant of gas A
N_A = flux of gas A within the pores of the particle
N'_A = flux of gas A within the pores of the reacted shell
P = defined by Eq. 35
R_o = radius of the particle
r = macroscopic radial distance in spherical coordinates
r' = microscopic radial distance in spherical coordinates
r_c = radius of unreacted shell
r_o = initial grain radius
S_v = grain surface area per unit volume of particle, defined in Eq. 2
$\mathcal{T}$ = time for complete conversion of grains at the surface
$\mathcal{T}_c$ = time for complete conversion of the particle
t = time
$\bar{t}$ = reciprocal time constant defined in Eq. 43
w = weight fraction of reactant solid B in sample
X = conversion of reactant solid B
Y = dimensionless microscopic radial coordinate
Y^* = Y at the surface of the particle
y_A = mole fraction of gas A in fluid M
y'_A = mole fraction of gas A in fluid F
$y_{A\infty}$ = mole fraction of gas A at the surface of the particle
Z = dimensionless macroscopic radial coordinate
Z^* = macroscopic moving boundary

Greek letters

α = function defined by Eq. 30
β = reciprocal time constant, $1/\mathcal{T}$
ϵ = porosity of the particles
ϵ' = porosity of the ash layer
η = defined in Eq. 14
θ = dimensionless time constant ratio defined in Eq. 22
μ_F = viscosity of fluid F, H_2SO_4 in this case (Table 1)
μ_M = viscosity of fluid M, H_2O in this case (Table 1)
ρ_B = density of reactant solid B
ρ_b = bulk density of the particles
τ = tortuosity of the pores within the particles
τ' = tortuosity of the ash layer
ϕ = function defined by Eq. 17
Ω = quantity defined in Eq. 12

Literature Cited

Abbasi, M. H., J. W. Evans, and I. S. Abramson, "Diffusion of Gases in Porous Solids: Monte Carlo Simulation in the Knudsen and Ordinary Diffusion Regimes," *AIChE J.*, **29**, 617 (1983).

Batarseh, K. I., "The Effect of Physical Properties of Toxic Mine Waste on Acid Mine Drainage: A Mathematical Model," MS Thesis, Dept. of Chemical Engineering, West Virginia Univ. (1987).

Bhatia, S. K., and D. D. Perlmutter, "A Random Pore Model For Fluid-Solid Reactions: I. Isothermal, Kinetic Control," *AIChE J.*, **26**, 379 (1980).

———, "A Random Pore Model For Fluid-Solid Reactions: II. Diffusion and Transport Effects," *AIChE J.*, **27**, 247 (1981).
Bischoff, K. B., "Accuracy of the Pseudo Steady State Approximation for Moving Boundary Diffusion Problems," *Chem. Eng. Sci.*, **18**, 711 (1963).
Carslaw, H. S., and J. C. Jäger, *Conduction of Heat in Solids*, Clarendon Press, Oxford (1959).
Crank, J., *The Mathematics of Diffusion*, Oxford Press (1975).
Davis, G. B., and A. I. M. Ritchie, "A Model of Oxidation in Pyritic Mine Waste: Parts 1 and 2," *Appl. Math. Modelling*, **10**, 314 (1986).
Evans, III, R. B., G. M. Watson, and E. A. Mason, "Gaseous Diffusion in Porous Media at Uniform Pressure," *J. Chem. Phys.*, **35**, 2076 (1961).
Gibson, J. B., and D. P. Harrison, "The Reaction Between Hydrogen Sulfide and Spherical Pellets of Zinc Oxide," *I&EC, Proc. Des. Dev.*, **19**, 231 (1980).
Haines, L. B., "The Effect of Iron Disulfide Size, Type and Morphology on the Production of Acid Mine Drainage," MS Thesis, Dept. of Geology, West Virginia Univ. (1986).
Hirschfelder, J. O., R. B. Bird, and E. L. Spotz, "The Transport Properties of Gases and Gaseous Mixtures: II," *Chem. Revs.*, **44**, 205 (1949).
Mason, E. A., A. P. Malinauskas, and R. B. Evans, "Flow and Diffusion of Gases in Porous Media," *J. Chem. Phys.*, **46**, 3199 (1967).
Perry, J. H., and C. H. Chilton, *Chemical Engineers' Handbook*, McGraw-Hill (1973).
Ramachandran, P. A., and L. K. Doraiswamy, "Modeling of Noncatalytic Gas-Solid Reactions," *AIChE J.*, **28**, 881 (1982).
Sandry, T. D., and F. D. Stevenson, "Molecular Conductance From a Curved Surface Through a Cylindrical Hole by Monte Carlo Methods," *J. Chem. Phys.*, **53**, 151 (1970).
Satterfield, C. N., *Mass Transfer in Heterogeneous Catalysis*, MIT Press (1970).
Szekely, J., J. W. Evans, and H. Y. Sohn, *Gas-Solid Reactions*, Academic Press (1976).
Szekely, J., and J. W. Evans, "A Structural Model for Gas-Solid Reactions with a Moving Boundary," *Chem. Eng. Sci.*, **25**, 1091 (1970).
Tseng, S. C., S. S. Tamhankar, and C. Y. Wen, "Kinetic Studies on the Reactions Involved in the Hot Gas Desulfurization Using a Regenerable Iron-Oxide Sorbent-II," *Chem. Eng. Sci.*, **36**, 1287 (1981).
Weisz, P. B., and R. D. Goodwin, "Combustion of Carbonaceous Deposits within Porous Catalyst Particles: I. Diffusion-Controlled Kinetics," *J. Cat.*, **2**, 397 (1963).
Wilke, C. R., and P. Chang, "Correlation of Diffusion Coefficients in Dilute Solutions," *AIChE J.*, **1**, 264 (1955).
Zoss, L. M., S. N. Suciu, and W. L. Sibbitt, "The Solubility of Oxygen in Water," *Trans. ASME*, **76**, 69 (1954).

Manuscript received May 24, 1988, and revision received Jan. 17, 1989.